Epitaxial growth of ultrathin palladium films on Re{0001}

Article

Accepted Version

The epitaxial growth of ultra-thin palladium films on Re{0001}

Haitham A. Etman, Zhasmina V. Zheleva, Georg Held and Roger A. Bennett[a]

School of Chemistry, University of Reading, Reading, RG6 6AD, UK

Ultra-thin bimetallic layers create unusual magnetic and surface chemical effects through the modification of electronic structure brought on by low dimensionality, polymorphism, reduced screening and epitaxial strain. Previous studies have related valence and core-level shifts to surface reactivity through the d-band model of Hammer and Nørskov, and in heteroepitaxial films this band position is determined by competing effects of coordination, strain and hybridization of substrate and overlayer states. In this study we employ the epitaxially matched Pd on Re{0001} system to grow films with no lateral strain. We use a recent advancement in low energy electron diffraction to expand the data range sufficiently for a reliable determination of the growth sequence and out-of-plane surface relaxation as a function of film thickness. The results are supported by scanning tunneling microscopy and x-ray photoemission spectroscopy, which show that the growth is layer-by-layer with significant core-level shifts due to changes in film structure, morphology and bonding.

---

[a] E-mail: r.a.bennett@reading.ac.uk, Telephone: +44 (0)118 378 8559

Keywords: Palladium, Rhenium, Structure, LEED-IV, thin film, Core-level shifts, STM, XPS

1. Introduction

Metallic thin films deposited on hexagonal single-metal crystals have received considerable attention in the past few decades[1,2] due to the interest in modifying the chemical, electronic and magnetic properties of the surface in a systematic and controllable manner. Such metal overlayers and surface alloys lend themselves to a variety of unusual catalytic properties such as facile H_2 dissociation and weak binding of CO which are beneficial in applications such as hydrogen fuel cells[3]. The most common substrate to be employed for the study of ultra-thin Pd films is the ruthenium {0001} surface which has an in plane lattice constant of 2.71Å. Pd layers grown on this surface are strained due to a lattice mismatch of circa 1.7% with respect to the Pd{111} in-plane spacing of 2.75 Å. In this study we employ the rhenium {0001} surface as a substrate due to its very close epitaxial match of the in-plane lattice constant of (2.76Å). With just 0.4% mismatch we expect epitaxial growth such that the surface defect density is low and as such the intrinsic properties of the Pd overlayer can be separated from variations induced by local perturbation of the lattice and strain. While the growth of Pd on Ru{0001} has recently been well characterized[4] there is a lack of similar quantitative structural data for the Pd on Re{0001} system.

Campbell *et al.*[5] studied the deposition of Pd on Re{0001} and Ru{0001} from sub-monolayer (ML) to multilayers using X-ray photoelectron spectroscopy (XPS) and temperature programmed desorption (TPD) employing CO and H_2 adsorption as probe molecules. They found a coverage dependent core level shift in the Pd $3d_{5/2}$ peak position (decrease in the binding energy as coverage increases) when deposited on Re{0001}. The peak shifts by ~ 0.15eV over the range 0.2ML to 1ML, after which a further continuous shift of 0.65eV was observed up to a coverage

of ~7ML. Beyond 7ML, no change in the peak position was observed up to 40ML Pd, the thickest films studied. TPD and XPS experiments on the adsorption of CO on 1 ML of Pd on Re{0001} revealed that the desorption temperature of CO from the system is ~ 110 K lower than that from Pd(100), indicating that Pd-Re interactions dramatically weakens the Pd-CO bond strength. These results were attributed to a charge transfer from the Pd adlayers to the Re substrate. Pick confirmed these results using self-consistent tight binding calculations of CO chemisorption on monolayer Pd deposited on Re{0001} and Ru{0001}[6]. Very recently Golfetto *et al.* [7] employed high resolution XPS to resolve Pd $3d_{5/2}$ core level shifts associated with the clean surface and Pd films on Ru{0001}. The results identified layer specific core level shifts which could be used as an experimental descriptor of chemical reactivity.

Several theoretical studies using density functional theory (DFT) have been performed on the 1 ML Pd on Re{0001} system. Wu and Freeman[8] have compared the bonding mechanism of Pd monolayers on various transition metals and showed that interfacial dipoles (i.e. charge polarisation induced in the Pd layer by the substrate) play a key role in the bonding mechanism. Charge accumulates in the interfacial region on top of the Re and is depleted from both Re and Pd atoms, which lowers the energies of the Pd states. They predict the hcp site to be preferred for 1 ML Pd on Re{0001}. Pallassana *et al.* [9] studied the chemisorption of hydrogen on the same surface and based their interpretation of the results on the d-band model developed by Hammer and Nørskov[10]. They related the weak chemisorption of hydrogen on 1 ML Pd on Re{0001} surface to a substantial lowering in the valence d-band centre of Pd by 0.72eV below that of the bulk Pd. This lowering was later confirmed experimentally by Mun *et al.*[2] who further suggested that the growth mode is of the Stranski-Krastanov type because of the manner in which the Pd $3d_{5/2}$ core level shifts and the peak shape changes as a function of coverage.

The rigid d-band model of Ruban *et al.* [11] predicts the d-band shifts in heteroepitaxial and surface alloy systems. The model uses changes in electron embedding density inferred from the elemental Wigner-Seitz radius and the local co-ordination of the substrate atom pair to predict core level shifts. While the model predicts the trend for Pd on Ru{0001}, for Pd on Re{0001} the Wigner-Seitz radius of both elements is identical and only a very small shift would be expected for unrelaxed surfaces[11]. In general, under-coordinated surface, step and kink atoms on transition metal surfaces (Pd[7,12], Pt[13], Rh[14]) consistently show lower binding energies with decreasing co-ordination, i.e. the opposite shift to the established experimental data for Pd on Re{0001}.

The physics of the modifications to the valence band structure of Pd to induce ferromagnetic order have lead to much interest in potential magnetic properties. A slight increase in the local density of states at the Fermi level is required to fulfill the Stoner criterion for ferromagnetism which may be brought about by growing strained layers, alternate polymorphs or nanoparticles[15]. In a DFT study of various Pd polymorphs, Hüger and Osuch[16] identified the onset of ferromagnetism with lattice expansion and showed thresholds at ~10% lattice expansion for fcc Pd, but that hcp and double-hcp (dhcp) are ferromagnetic at the optimum bulk lattice spacing (which was identical for all polymorphs). Hüger and Osuch also experimentally attempted to grow hcp structures on W(100) and reported flat bands in angle-resolved UPS near the Fermi level implying that Pd becomes ferromagnetic. More recent DFT calculations by Alexandre *et al.*[17] predicted that bulk Pd in hcp structures to be ferromagnetic and the fcc phase paramagnetic. However, two dimensional defects, such as surfaces, twin boundaries and stacking faults with locally hcp stacking in an fcc lattice increased the magnetic susceptibility. The (111) surface is paramagnetic, but has a large susceptibility, and was suggested to have a propensity to become

magnetic if in close proximity to stacking faults. The stacking sequence and structure is clearly of relevance to a detailed understanding of magnetism in Pd thin films.

No experimental structural analysis of Pd/Re{0001} has been published (in contrast Pd/Ru{0001} has been studied by de Siervo *et al.*[18] and later by Santos *et al.*[4]). In this study we present the first detailed structural analysis of ultra-thin Pd films on Re{0001} in the range 0 - 4 ML investigated by a combination of quantitative LEED, scanning tunneling microscopy (STM) and XPS. We show that Pd grows epitaxially with the first layer following the hcp sequence of the substrate and subsequent layers growing in fcc structure. The use of non-normal incidence data in LEED structural analysis beams allows a far greater effective range of useful energies to be considered.

2. Experimental Procedures and Structure Analysis

2.1. Experiment

The experiments were undertaken in a twin UHV chamber system described in detail previously[19,20] which has now been modified to incorporate a small scanning tunneling microscope operating at room temperature with an associated sample transfer system. The preparation chamber is equipped with a Vacuum Generators 3 grid low energy electron diffraction (LEED) system with a 16 bit peltier cooled ccd camera to capture LEED images and an Oxford Applied Research water-cooled e-beam evaporator for Pd deposition. XPS was performed in a mu-metal analyser chamber equipped with a hemispherical analyser and an unmonochromated Al Kα X-ray source (hν = 1486.6 eV). Binding energies are referenced to the Re 4f7/2 at 40.2eV with positions assigned on the basis of mixed Gaussian-Lorentzian product peakshape on a Shirley background. The homemade STM is mounted in a six-way cross on the analyser chamber and operates in UHV at room temperature with mechanically cut

platinum/iridium (Pt80/Ir20) tips. The STM is controlled by an Oxford Instruments TOPS III system. Lateral length scales were calibrated by atomic resolution imaging of a c(6×2) oxide superstructure on Cu{110} resulting in a largest scan size of 8000Å. The z-scale is calibrated from the images of the clean Re surface reported here. Single crystals are held in place by Ta sheet or W wire inserted into a narrow slit around the crystal perimeter and spotwelded to tantalum sample plates. These plates are transferred from the STM to the main analysis chamber transfer arm for e-beam heating, cleaning, deposition, XPS and LEED analysis. Sample temperatures were initially calibrated and measured by a c-type thermocouple spot welded on the side of the crystal but the thermocouple was later removed to aid sample transfer. Temperatures were subsequently inferred from measurements of heating power employed and the previous calibration data.

The sample is cleaned by repeated cycles of flash heating to ~ 2300 K, followed by a short anneal at ~ 1300 K in 5×10^{-8} Torr O_2 for ~ 20 minutes to remove carbon, the initial primary contaminant, and then flashed to desorb oxygen. This cycle was repeated until the LEED pattern indicated a well-ordered (1×1) hexagonal surface and the XPS showed a clean surface. To remove all oxygen two final flashes were found to be necessary. Pd was deposited at ~ 0.7 ML/min onto the Re surface as it cooled to RT (typically about 373K) with no post deposition anneal. The Pd flux was monitored using the ion current meter integral to the source (typically ~12nA) which also takes a high fraction of the charged Pd from the beam (reducing the possibility that these influence the growth mode significantly). The flux was calibrated using the photoelectron intensity of the Pd 3d peaks (measured at 50eV pass energy) as a function of time to identify monolayer break points.

LEED-IV experiments were performed on the clean surface using three angles of incidence (polar angles of +3°, -7° and +10°) in the energy range of 75 – 300 eV and on the 1, 2, 3 and 4 ML Pd films using two angles incidence (normal and 10^{o} off-normal) in the energy range of 50 – 255 eV. At normal incidence, all the spots of the same order are equivalent and were therefore averaged[21] (i.e. 3 sets of spots are being used for normal incidence (1, 0), (1, 1) and (2, 0) plus 18 for the off-normal data with the calculations run simultaneously). The LEED patterns were all of high intensity with a low background and did not contain any superstructure spots. Stray light from the electron gun was background subtracted from each 16-bit image. The total energy ranges for the analysis were 7040eV for the clean surface and between 1670 and 1900eV for each of the films.

2.2. LEED-IV Calculations

The program used to compare the theoretical and experimental intensity versus electron energy (IV) curves is CLEED[22]. The LEED-IV calculations[23] are based on fully dynamical scattering theory described by Pendry[24] and Van Hove and Tong[25]. Technical details and a full set of resulting data are given in Supplementary Information[26]. The agreement between the experimental and theoretical IV curves was quantified with Pendry's R_P factor and the error limits for the determined parameters were calculated using the RR factor method[27]. In all calculations a (1×1) periodicity was assumed. The angle of incidence was optimized as part of the structural optimization, which increases the number of search parameters by 2.

A recent modification to the program allows for the simultaneous fitting of multiple data sets acquired from the same sample at different angles of incidence. The breaking of symmetry, in comparison to experiments with carefully aligned normal incidence, allows an effective increase of the energy range as LEED spots are no longer symmetrically equivalent. Thus more complex

structural models can be addressed; in this case surface structures with inequivalent domains mixing spot intensities.

3. Results and discussion

3.1. Clean Re{0001} structure

The Re{0001} surface is the most stable truncation of the crystal and exhibits large terraces. STM images of the clean surface, Figure 1, show single steps separating terraces of width ranging from 150 to 860Å. The average single step size was used to calibrate the z-scale of the STM to be consistent with the interlayer spacing for the Re{0001} surface ~2.3Å within small error margins. The step edges are extremely well defined and straight over extended distances. We did not achieve atomic resolution on the clean surfaces so cannot be explicit in assigning the direction of the steps but we expect them to run in the close-packed directions .

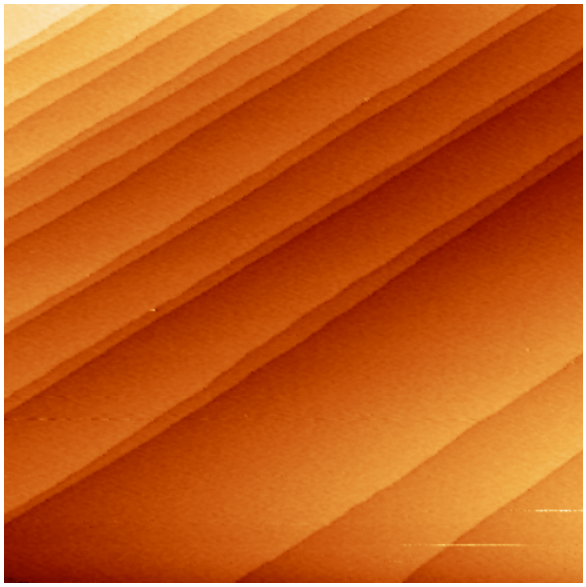

Figure 1. (3000Å × 3000Å) STM image of clean Re{0001} surface taken at 0.1nA tunelling current and 1V bias voltage showing wide terraces and straight monatomic step edges.

An ideal step free {0001} basal plane of an hexagonal close packed surface has threefold symmetry, however, on examining the surface using conventional LEED, a sixfold symmetric

pattern is observed at normal incidence. Figure 2 explains how this pattern is generated by the presence of monatomic steps at the surface which introduce two types of terraces, A-terminated and B-terminated (where A and B represent the two possible terminations of the hcp stacking sequence). The diffraction pattern from both terrace types is three-fold symmetric but each is a mirror image (or rotated by 180°) [28] with respect to the other, resulting in each LEED spot being an incoherent sum of diffraction intensities from both terraces.

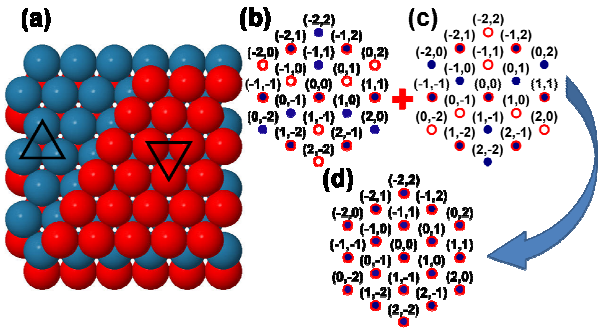

Figure 2. (a) hard sphere model of the hcp {0001} surface with a monoatomic step between an A- and B-terminated terrace; different colours represent atoms in A and B layers. The triangles surrounding hcp hollow sites (above a second layer atom) indicate that the terraces are mirror images of each other. (b) and (c) schematic LEED patterns of the A- and B-terminated terraces; filled and open circles represent spots related by the surface symmetry. Symmetry-related spots of the same order (distance from the specular (0,0) spot) have the same LEED-IV curves if data are taken at normal incidence. (d) Superposition of the LEED patterns from both terraces representing the six-fold symmetry observed in the experiment at normal incidence.

For the {0001} basal plane the terraces are degenerate in energy and are expected to occur with equal abundance at thermodynamic equilibrium on the surface. The LEED-IV data are therefore an average over the two terrace types. Figure 2b-d show how diffraction patterns

generated by each terrace (filled and open circles) add to give a 6-fold symmetric LEED pattern at normal incidence. In Figure 3 we show sample LEED-IV data taken at 3° off normal and at larger angles (-7° and +10°) from the clean surface. The left and right panels show the results for (-1,0) and (0,-1) first order LEED spots, respectively. At 3° off normal incidence they are very similar (but not identical), however, for increasing angles away from normal incidence large differences emerge. This is because the symmetry of the diffraction geometry is broken at off-normal incidence and features from different terraces become inequivalent. Some of the terraces shown in Figure 1 are separated by closely bunched steps and some of these terraces are therefore relatively small leading to a local bias in step termination (more A terrace than B). However, this is a very small sample area in comparison to that measured by conventional LEED and we expect local biases on small lengthscales in step termination to cancel out, and indeed later STM images of Pd coated surfaces bear this out.

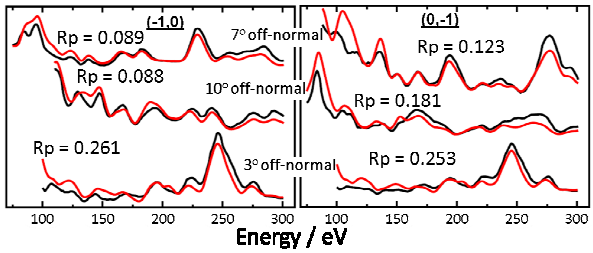

Figure 3. Sample LEED-IV curves for two spots representing the two types of terraces, (-1,0) on the left and (0,-1) on the right, with Pendry's R-factors (R_P). Black lines represent experimental curves and red lines represent theoretical fits. At 3° incidence both (-1,0) and (0,-1) have similar structure. Further off normal the curves for each spot look dissimilar as the symmetry is broken and the curves contain independent information.

Following from the above model, the surface structure of the inter-layer spacing of the top four atomic layers was determined by simultaneously fitting models for the three angles with the

assumption that there was no dominant terrace type on the surface (i.e. a 1:1 mix of A and B terminations). The best R_P -factor obtained is 0.155 for a relaxed structure of the clean surface, a summary of the results is shown in Table 1. The pattern of surface relaxation (a top layer contraction, second layer slight expansion and third layer small contraction) is common to most metal surfaces[29]. The experimental results are smaller in size, however, than the large relaxations predicted theoretically for the outermost atoms of this surface[8,9].

Table 1. Summary of LEED-IV results obtained for the clean surface

Polar Angle	3.11 ± 0.12°	9.93 ± 0.05°	6.94 ± 0.09°
Azimuthal Angle	176.06 ± 0.06°	102.81 ± 0.08°	238.98 ± 0.1°
R_P	0.158	0.132	0.167
RR	0.112	0.117	0.123
Energy Range / eV	2573.0	2341.25	2126.25
Average R_P	0.152		
Average RR	0.067		
Total Energy Range / eV	7040.5		
Interlayer separation	Experiment	Theory	
d_{12} / Å	2.13 ± 0.02 (-4.3 ± 0.8%)	2.07 (-7.4%)	2.06 (-7.6%)
d_{23} / Å	2.28 ± 0.02 (+2.3 ± 0.8%)	2.32 (+3.9%)	2.28 (+2.3%)
d_{34} / Å	2.19 ± 0.02 (-1.7 ± 1%)	bulk	-
d_{45} / Å	2.20 ± 0.03 (+1.3 ±1.5%)	From ref [6]	From ref [8]
d_{bulk} / Å	2.23		

3.2. Ultra-thin Pd Films

3.2.1. XPS and Core-level shifts

The Pd 3d photoemission was monitored as a function of deposition time to establish a calibration curve for the evaporator flux as shown in Figure 4. Figure 4a shows the Pd $3d_{5/2}$ region for a succession of different coverages, while Figure 4b shows the aggregated intensity of the entire Pd 3d photoemission. The clear break points in the Figure 4b intensity vs. flux curves immediately suggest a layer by layer growth mode for at least the first two monolayers, as expected for an epitaxial system with very little strain. We assign the breaks at 780 nA.s and 1600 nA.s to the completion of the first and second monolayers, respectively.

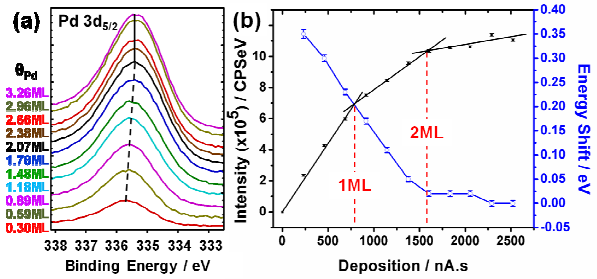

Figure 4. Core-level shifts for Pd $3d_{5/2}$ XPS signal (a) XPS signal of various coverages with black dotted line showing shift in peak position and the solid one showing no shift for higher coverage (b) Calibration of the coverage by monolayer break point analysis of the intensity of Pd 3d signal versus deposition time multiplied by evaporator ion flux and a plot of the Pd $3d_{5/2}$ core level shift (from 335.69eV to 335.34eV) as a function of increasing Pd deposition.

While synchrotron radiation studies have managed to resolve the Pd $3d_{5/2}$ peak into multiple components[1], here we work with an unmonochromated X-ray source and we resolve one broad peak which shifts systematically as a function of layer thickness. In figure 4b we show a continuous shift in binding energy from 335.69eV at approximately 0.30ML to 335.36eV at the completion of 2ML and then a very slow and small change to 335.34eV over the next monolayer. The uncertainties in the core-level shifts were determined using the in-built Monte Carlo

simulation function in CasaXPS[30] and were found to be of the order of a few mV (including uncertainties in the Re $4f_{7/2}$ reference energy assignments). Previous work by Goodman shows a similar change in binding energy over a larger range of coverage (in that work the coverage was determined calibrating to an assumed Pd ML temperature programmed desorption peak and not directly as here).[5]

3.2.2. Scanning Tunneling Microscopy

The deposition of Pd films was studied using STM from submonolayers to just above 1ML. The STM images, Figure 5 support the interpretation of the growth mode to be layer by layer. For submonolayer deposition of ~ 0.25 ML Pd onto a room temperature substrate the Pd forms fractal islands on the terraces which do not appear to preferentially wet the step edges as shown in Figure 5a. Similar islands have been observed before in homo and heteroepitaxial growth, and form due to diffusion-limited aggregation[31,32]. At higher coverage, as shown in Figure 5b, these islands connect and fill in to form more compact islands losing their fractal shapes as the fractal "branches" thicken. They do not, however, form compact islands as the island peripheries remain strongly structured with a lack of straight steps leading down to the Re terrace. The islands are of a single Pd layer height (i.e. they wet the surface rather than growing as multilayered islands). The Pd islands contact the straight Re step edges as they grow, however the step edge is still distinguishable as a straight feature between the islands. At the completion of 1ML, almost the whole surface is covered with Pd leaving just a small part of the surface not covered, which is a normal phenomena observed even in homoepitaxial growth of metals. In Figure 5c and 5d, a 1.25ML Pd film was grown and we can immediately see that most of the surface is covered before the second layer starts to grow (~ 7% of the Re surface is not covered). The film tends to extend across the terraces but stops at the step-edges and so reproduces the

underlying Re straight step structure. However, it is apparent that regions growing alongside the small amount of uncovered Re still maintain the heavily structured Pd down to Re step geometry as seen in Figure 5b. Pd growing as a second layer on the film forms compact islands with approximately hexagonal structure as expected for (111) oriented structures. There is little tendency to connect directly to the neighbouring step edges and most second layer Pd appears in the middle of the terraces. Of the islands which do appear to be growing from the step edges onto the terrace a minority appear to be continuous and most of them have a grain boundary or discontinuity at the interface.

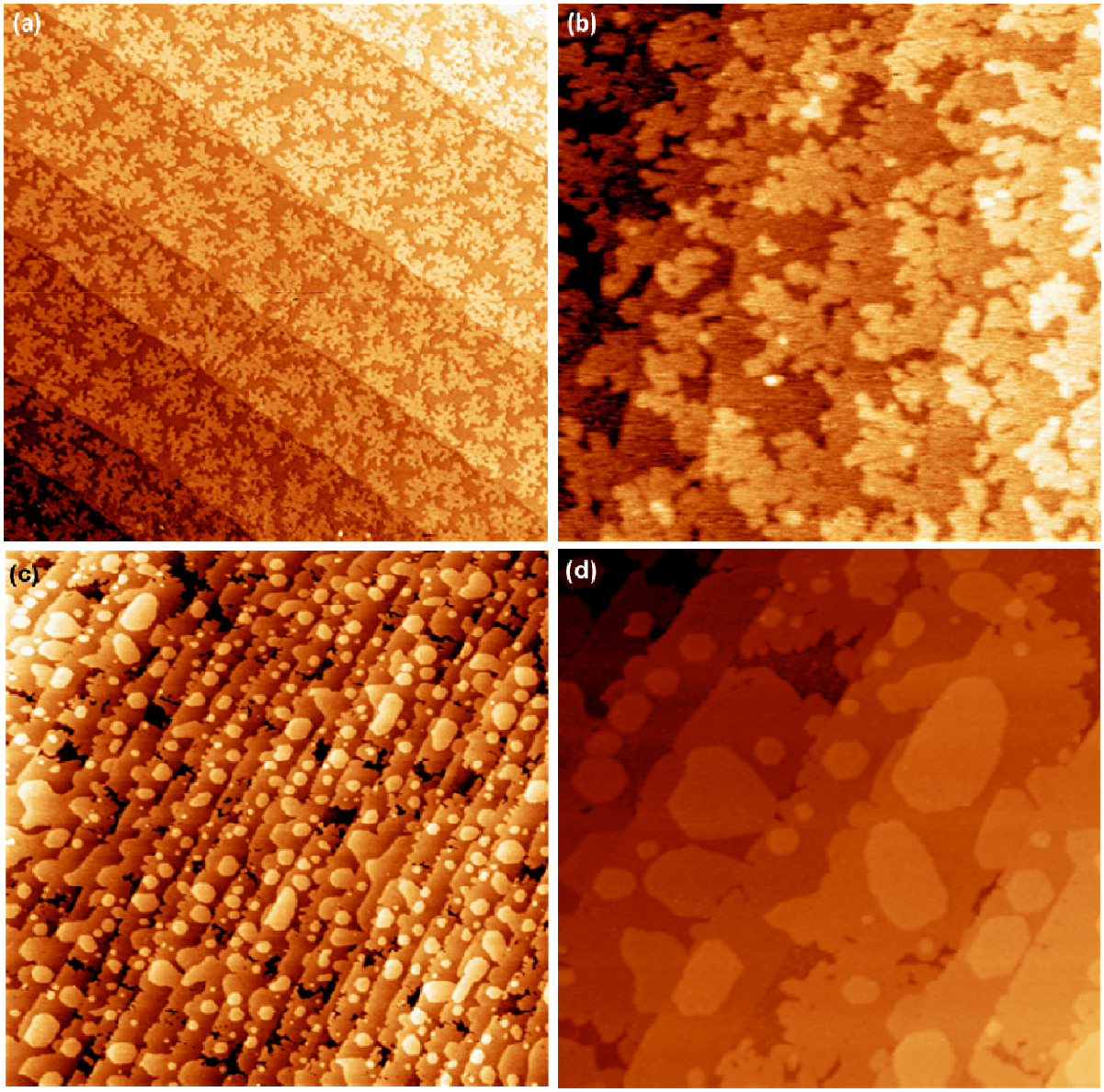

Figure 5. STM images of multiple Pd coverage on the surface: (a) (2700Å × 2700Å) image taken using 0.1nA tunneling current and 2V bias voltage of ~0.25ML fractal islands that do not wet the step edges. (b) (1130Å × 1130Å) image taken using 0.1nA and -1V of ~0.4ML compact islands of Pd with no visible straight step edges. (c) (4440Å × 4440Å) image taken using 0.5nA and 2V of ~1.25ML Pd (d) (1500Å × 1500Å) taken using 0.5nA and 2V bias voltage of ~1.25ML Pd layers.

In Figure 6 we show a closer examination of the islands and films on the terraces along with line profiles across features of interest. We can also report that the STM imaging reveals a distinction between Pd monolayer and the Re substrate on the next terrace up (i.e. in the same crystal plane); the Pd tends to image with an apparent height higher than the neighbouring Re due to a chemical contrast. We did not find, however, that this contrast was particularly sensitive to the tunneling conditions employed. In Table 2 we present the measured apparent heights from the STM images along the same profile taken across three images of the same area. The clean Re-Re step height images as ~2.2 Å for most images as expected as this measurement should not show any chemical contrast. The 1 ML Pd apparent height is measured from Re substrate to the edge of the film and has a chemical difference between Re and Pd and a small contrast difference with tunnel current. The 2 ML Pd height is the apparent height of an island on a 1 ML Pd film on a terrace and may have contrast differences in the electronic structure of 1 and 2 ML thick films. The final contrast occurs where a Pd film on a lower terrace meets a clean Re upper terrace (i.e. the terrace switches from Re to Pd termination), in which case the Re appears at significantly lower apparent height than the Pd.

Table 2. Dependence of apparent height of surface structures on tunneling condition.

Sample Bias / V	+2.0	-2.0	+2.0
Tunnel current / nA	1.0	1.0	4.0
Re - Re step / Å	1.98	2.17	2.17
1ML Pd - Re / Å	2.71	2.25	2.19
2ML Pd - 1ML Pd / Å	2.10	2.32	2.04
1ML Pd - Re in plane / Å	0.80	0.66	0.68

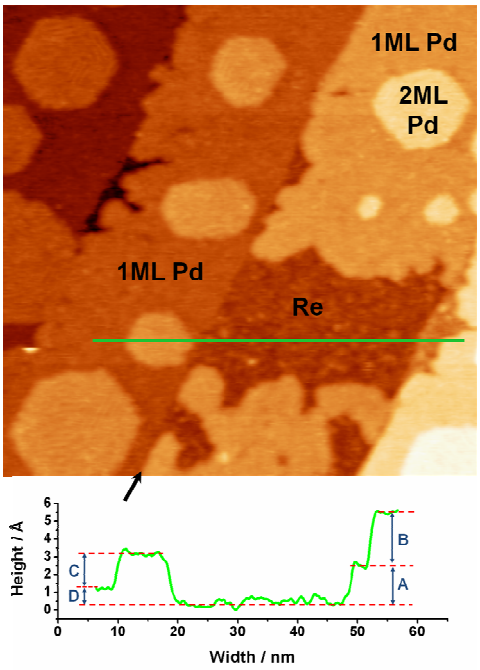

Figure 6. (640Å × 640Å) STM image of 1.25ML Pd deposited on the surface. The arrow points along the straight step edge of the substrate. The line profile shows the heights of the different features on the surface: (A) is the Re – Re step height, (B) 1ML Pd – Re, (C) 2ML Pd - 1ML Pd and (D) 1ML Pd - Re in plane. The values are given in Table 2.

3.2.3. LEED-IV analysis

Pd was deposited at just above room temperature (sample had cooled from the flash desorption of oxygen to < 373K) to form ultra-thin films of thickness of 1, 2, 3 and 4ML. Each layer was examined using LEED-IV. The pattern observed was a (1×1) hexagonal pattern qualitatively the same as the substrate, suggesting a pseudomorphic growth. Since the LEED images showed a hexagonal pattern and the lattice mismatch between Pd and Re is negligible (~0.4%), a hollow site would be the most obvious adsorption site for the first layer of Pd atoms. These may adopt an hcp stacking sequence (adatom above a second layer substrate atom) or an fcc structure (adatom above an empty substrate site in the second layer). Subsequent layers may introduce

stacking faults or continue to grow as substrate layers (or could potentially re-arrange the previous layer). Thus multiple layer stacking leads to a plethora of different models. A comprehensive trial of possible models was undertaken for each film, including differing film thicknesses to probe our sensitivity to systematic errors in coverage calibration. Table 3 shows the models with their resulting R_P and RR factors. The lowest R_P factors are all below those reported for atomic adsorbates, such as S on Re{0001}[33]. Competing models with similar R_P can be distinguished by evaluating the upper limit $R_{Pmax} = (1+RR)\times R_{Pmin}$ (where R_{Pmin} is the lowest R-factor). If a trial model has an R_P factor higher than R_{Pmax} then it is statistically unlikely and can be ignored. The R_P factors within the statistical error margin of R_{Pmin} are printed in bold characters.

Table 3. Summary of attempted models with their associated R_P and RR factors[b]

No. of ML	Stacking Sequence	R_P	RR	No. of ML	Stacking Sequence	R_P	RR
1	ABABA	0.574	0.112	3	ABAB*cbc*	0.420	0.133
	ABAB*a*	**0.218**	**0.112**		ABAB*abab*	0.412	0.133
	ABAB*c*	0.465	0.112		ABAB*abac*	0.332	0.133
	ABAB*ab*	0.462	0.112		**ABAB*abca***	**0.272**	**0.133**
	ABAB*ac*	0.562	0.112		ABAB*abcb*	0.408	0.133
	ABAB*ca*	0.573	0.112		ABAB*acab*	0.343	0.134
	ABAB*cb*	0.510	0.112		ABAB*acac*	0.408	0.133
2	ABAB*a*	0.577	0.121		ABAB*acba*	0.310	0.134
	ABAB*c*	0.561	0.121		ABAB*acbc*	0.402	0.133
	ABAB*ab*	0.351	0.121		ABAB*caba*	0.406	0.133
	ABAB*ac*	**0.211**	**0.121**		ABAB*cabc*	0.312	0.134
	ABAB*ca*	0.268	0.121		ABAB*caca*	0.410	0.133
	ABAB*cb*	0.386	0.121		ABAB*cacb*	0.349	0.133
	ABAB*aba*	0.380	0.121		ABAB*cbab*	0.410	0.133
	ABAB*abc*	0.324	0.121		**ABAB*cbac***	**0.270**	**0.133**
	ABAB*aca*	0.410	0.121		ABAB*cbca*	0.343	0.133
	ABAB*acb*	0.353	0.121		ABAB*cbcb*	0.420	0.133
	ABAB*cab*	0.366	0.121	4	ABAB*aca*	0.464	0.127
	ABAB*cac*	0.425	0.121		ABAB*acb*	0.243	0.127

[b] The uppercase and lowercase letters represent the substrate and the Pd overlayer, respectively. Fits within the error margins defined by RR are highlighted in bold with the best solutions underlined

	ABAB*cba*	0.312	0.121		ABAB*acab*	0.288	0.127
	ABAB*cbc*	0.375	0.121		ABAB*acac*	0.475	0.128
	ABAB*ab*	0.388	0.133		**ABAB*acba***	**0.209**	**0.127**
	ABAB*ac*	0.302	0.133		ABAB*acbc*	0.446	0.128
	ABAB*ca*	0.284	0.133		ABAB*acaba*	0.440	0.127
	ABAB*cb*	0.400	0.133		ABAB*acabc*	0.239	0.127
	ABAB*aba*	0.419	0.133		ABAB*acaca*	0.458	0.128
3	ABAB*abc*	0.284	0.133		ABAB*acacb*	0.281	0.127
	ABAB*aca*	0.404	0.133		ABAB*acbab*	0.433	0.127
	ABAB*acb*	**0.248**	**0.133**		**ABAB*acbac***	**0.225**	**0.127**
	ABAB*cab*	**0.275**	**0.133**		ABAB*acbca*	0.283	0.127
	ABAB*cac*	0.396	0.133		ABAB*acbcb*	0.465	0.128
	ABAB*cba*	0.303	0.133				

The first result to note is that the best fit structures are always for models with the same number of Pd layers as expected from the experimental deposition times. This again leads to a high confidence that the layers are growing layer by layer and that our XPS derived monolayer breakpoint analysis is correct. For 1 and 2ML films the models leading to R_{Pmin} are clearly outside the statistical error bar of any other structure and represent exactly the expected film thickness. For thicker films competing models with similar R_P can be distinguished by evaluating the upper limit R_{Pmax} (see above). The 3ML models ABABcab, ABABabca, ABABcbac (R_P = 0.275, 0.272, 0.270) are within the statistical margin of the best fit model ABABacb (R_P = 0.248) and the 4ML model ABABacbac (R_P = 0.225) competes with the best fit structure ABABacba (R_P = 0.209). All other models fall outside R_{Pmax} criterion.

The best results obtained suggest a growth model in which the first layer adopts an hcp pseudomorphic structure ABAB*a*; the second layer introduces a stacking fault to give a fcc like termination ABAB*ac*; with subsequent layers growing in an fcc pattern to give a stacking sequence of ABAB*acba*. This model is also consistent with what was found for the more complex epitaxially strained growth of Pd on Ru{0001} by LEEM/LEED on a single terrace[28]. The 3ML ABAB*cab*, ABAB*abca,* ABAB*cbac* and 4ML ABAB*acbac* structures were, however, competitive at this level with the lowest R_P structures. These models were carried forward for a final refinement by optimizing the non-structural parameters: (a) Debye-Waller factor; (b) real and imaginary part of the optical potential. In doing this we found these competing trial structures resulted in R_P values of 0.202 (ABABacb), 0.234 (ABABcab), 0.231 (ABABabca) and 0.232 (ABABcbac) for the 3ML models, and 0.152 (ABABacba) and 0.191 (ABABacbac) for the 4ML structures. This eliminates all but the ABABacb and ABABacba models for the 3ML and 4ML data, respectively. Details of these structures are listed in Table 4.

To test the possibility for in-plane relaxation into the bulk Pd structure of the thickest (4ML) films the same models were run using Pd lateral unit cell dimensions instead of Re. The resulting R_P for 4ML ABAB*acba* and ABAB*acbac* are 0.204 and 0.223, respectively, which are again worse fits than for the best structures of Table 4. We therefore conclude that the growth is predominantly layer by layer, and that the films grow to form an ABAB*acba* stacking sequence in single domains of fcc on each terrace with the Re in-plane lattice constant. Some example LEED-IV curves for 1-4ML thick films are shown in Figure 7.

Table 4. Summary of LEED-IV results obtained for the interlayer spacing of 1-4 ML Pd films[c] with comparison to reference [9] for 1 ML DFT results.

No. of ML	1	2	3	4
Structure	ABAB*a*	ABAB*ac*	ABAB*acb*	ABAB*acba*
Rp	0.187	0.180	0.202	0.152
RR	0.132	0.130	0.139	0.137
Energy Range	1844.00	1906.25	1668.00	1705.50
d_{12} / Å	***2.20 ± 0.05*** ***(-1.9 ± 2.3%)*** ***2.252 (+0.9%)***[9]	2.30 ± 0.04 (+2.5 ± 1.6%)	2.34 ± 0.04 (+4.3 ± 1.9%)	2.30 ± 0.03 (+2.5 ± 1.4%)
d_{23} / Å	2.18 ± 0.03 (-2 ± 1.4%) 2.152 (-3.5%)[9]	***2.23 ± 0.03*** ***(-0.5 ± 1.6%)***	2.29 ± 0.04 (+1.7 ± 1.7%)	2.28 ± 0.03 (+1.6 ± 1.2%)
d_{34} / Å	2.25 ± 0.04 (+0.8 ± 1.7%) 2.275 (+2.0%)[9]	2.19 ± 0.07 (-1.8 ± 3%)	***2.28 ± 0.07*** ***(+1.4 ± 3%)***	2.30 ± 0.05 (+2.3 ± 2.3%)
d_{45} / Å	2.23 ± 0.06 (-0.1 ± 2.7%) bulk[9]	2.30 ± 0.07 (+3.4 ± 3%)	2.17 ± 0.13 (-2.6 ± 5.9%)	***2.30 ± 0.06*** ***(+2.3 ± 2.8%)***

[c] The layer spacing is both absolute distance and as a percentage of the bulk interlayer spacing, with a negative value being a contraction. The italicized entries are at the Pd-Re interface with the bulk value averaged over the Pd-Pd(111) bulk and Re-Re{0001} bulk inter-layer separations.

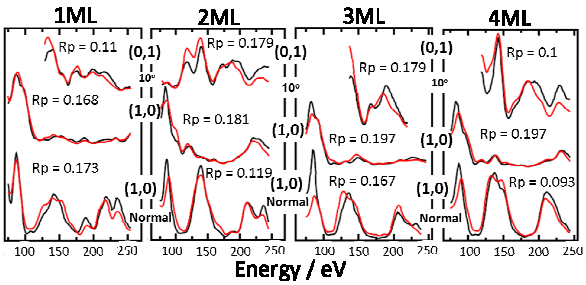

Figure 7. Sample LEED-IV curves representing 1-4ML Pd deposited on Re{0001} at two angles; Normal incidence and 10° off-normal. Black curves represent the experimental data and red curves represent the theoretical fits along with R_P for each pair. The full set of LEED-IV curves are shown in Supporting Information[26].

4. Discussion

The LEED-IV results show that the outermost Re layer tends to remain slightly contracted as Pd layers grow on top. For the 1ML film the Pd-Re layer spacing of 2.20 ± 0.05Å compares favorably with the calculated values of 2.18Å by Wu and Freeman[8] and 2.252Å of Pallassana *et al.*[9] On the clean surface and for electronegative adsorbate layers, such as S, significantly larger contractions are observed with d_{12} distances ranging from 2.08Å (0.25ML S [33]) to 2.13Å (clean surface) or -7 to -4 %. This points towards charge transfer from Pd to Re, as expected, at the interface. The 1ML data also indicates that the surface relaxation of the first Re-Re layer is not entirely lifted by the adsorption of Pd which correlates well with the theoretical work of Pallassana *et al.*[9].

The Pd-Pd inter-layer spacing for all multilayer films are expanded with respect to their bulk inter-layer spacing. This is a similar, but smaller, effect than that described by de Siervo *et al.*[18] for the strained 5 ML Pd/Ru{0001} system who suggest strain from island and domain formation is responsible for the lattice expansion. The Pd interlayer spacings of the thickest film here are,

however, within experimental error the same as those reported by Van Hove's group for Pd(111) single crystals, which show approximately 1 ± 2% expansion of the outermost d_{12} separation[34]. The origin of this expansion is the cause of some controversy in the literature as hydrogen incorporation into Pd bulk leads to a lattice expansion, so one argument is that hydrogen from residual gas in UHV could be responsible. However, it is often found theoretically that the outer layers of Pd bulk are expanded, with DFT calculations[9] predicting a d_{12} separation of 2.315Å (+3.1%). Hydrogen chemisorption on the 1 ML Pd/Re{0001} is predicted to cause large expansions of the outermost d_{12} separation to 2.304Å from 2.252Å for the clean film surface[9].

The main result of the LEED-IV study is, however, to determine the stacking sequence of the film as it grows as this information cannot be reliably retrieved by scanning tunneling microscopy. As the film grows it sequentially adopts an ABAB*acba* stacking sequence and the fcc film grows in a single orientation dictated by the terrace upon which it nucleates. Films nucleated on the alternate terrace adopt a similar fcc stacking sequence but, due to the alternating layers in the hcp substrate, induce a stacking fault at the substrate step edge in 2 ML or greater film thicknesses. So despite a near perfect epitaxial match of nearest neighbor distances between overlayer and substrate our films are not necessarily strain and defect free. We predict that for thicker films the stacking faults induced by the substrate steps will adopt low energy configurations and may be a useful method of inducing a known defect structure into unstrained fcc bulk materials. The scanning tunneling microscopy results of Figure 5c and 5d show this effect clearly as relatively little Pd in the second layer wets the step edges and prefers to decorate the terrace. The growth of the first Pd monolayer is also interesting as this adopts the substrate hcp structure and as such should not generate a stacking fault at the step edges. Again, however, the Pd avoids the step edges with most of the material forming fractal structures on the terrace at

very low coverage, Figure 5a, and more compact but still dendritic structures with increased coverage, Figure 5b.

The low average coordination of submonolayer Pd at the Re{0001} surface would be expected to induce core-level shifts to lower binding energy, however, we see the opposite effect. The strong binding of Pd to Re, and the fact that the Pd is sitting in hcp sites of the surface in preference to the usual fcc structure[8], induces a very significant charge transfer from the low co-ordination Pd. This strong interaction broadens the surface atom d-bands[9] and shifts the valence and core levels to higher binding energy in XPS. As the average coordination increases with coverage towards completing a full layer (the fractal islands fill in) the changes in local environment move the peak towards the bulk position. Structural relaxations have also been noted to cause small corrections to binding energy shifts predicted on the basis of coordination in experiment[35] and theory[11]. The LEED-IV from multilayer films indicate the initial Pd contraction relaxes into an expansion and so may be expected to yield a shift of the states to lower binding energy. Eventually we have a three layer system with a wide d-band positive core-level shifted Pd layer at the interface buried beneath a bulk like Pd with an outer surface which is expected to show a negative binding energy shift due to under-coordination and slightly narrower bands. The low resolution XPS data however preclude detailed examination of the layer by layer core level shifts but both the magnitude and sign are comparable to the existing literature. Our shift occurs over a much narrower coverage range than hitherto reported (2ML here versus 5-7 ML in refs [2] and [5] respectively) as would be expected for a chemical bonding effect localized at the interface. We conclude that the strong interaction of Pd and Re lead to chemical ligand effects that out compete the opposing shifts induced by low coordination. These effects diminish with coverage by 2 ML as the second monolayer covers the first.

5. Conclusion

The Re{0001} surface has been employed as a substrate for the unstrained epitaxial growth of Pd ultra-thin films. The use of multiple angle simultaneous LEED-IV structural refinement enabled reliable surface structure determination in the presence of two terrace types. The growth of 1-4 ML Pd thin films on the Re{0001} surface was investigated by LEED-IV, XPS, and STM. LEED-IV showed the film to follow ABAB*acba* stacking sequence with thicker layers expanding with respect to Pd bulk inter-layer spacing. 1 and 2 ML films display a contraction at the Pd-Re interface due to the strong chemical interaction of the metals. The trend in the core level shifts towards a lower binding energy with increasing coverage agrees with the experimental literature, however, our shift occurs over a much narrower coverage range than reported hitherto. The out of plane contraction of the films is reduced with increasing thickness, and the outer layers expand with respect to bulk Pd values. STM images of submonolayer coverage show fractal islands that do not cover any steps at 0.25ML which change to more compact islands at 0.4ML. At 1.25ML the islands formed are of hexagonal shapes with at least 93% of the surface covered before the second layer starts to grow. Step edges show different structures for the 1 ML Pd and the 2 ML Pd, the former being much more irregular than the close packed structures of the latter. The structural data, stacking sequence, and correlation of the core level shifts with well characterized film thickness will inform theoretical and experimental work on the heteroepitaxial growth of Pd, and for Pd coated nanostructured catalysts. We hope to make detailed measurements of the core-level fine structure in future.

Acknowledgment

We thank Grongar Lloyd and Richard Palmer at the University of Birmingham, UK for the permanent loan of the STM. H.A.E. and Z.V.Z. acknowledge the EPSRC and the ‘‘Research

Endowment Trust Fund'' of the University of Reading for postgraduate studentships, respectively. We thank the Royal Society / Wolfson Foundation for laboratory refurbishment grant and Alan Adams for engineering the sample transfer system.

Supporting Information Available

This information is available free of charge via the Internet at http://pubs.acs.org.

References

1 Hwang, R. Q.; Bartelt, M. C. *Chem. Rev.* **1997**, *97*, 1063

2 Mun, B. S.; Lee, C.; Stamenkovic, V.; Markovic, N. M.; Ross Jr, P. N. *Phys. Rev. B* **2005**, *71*, 115420

3 Greeley, J.; Mavrikakis, M. *Catal. Today* **2006**, *111*, 52.

4 Santos, B.; Puerta, J. M.; Cerda, J. I.; Herranz, T.; McCarty, K. F.; de la Figuera, J.; *New J. Phys.* **2010**, *12*, 023023

5 Campbell, R. A.; Rodriguez, J. A.; Goodman, D. W. *Phys. Rev. B* **1992**, *46*, 7077

6 Pick, S. *J. Phys. Chem.* **1995**, *99*, 15375

7 Golfetto, E.; Baraldi, A.; Pozzo, M.; Alfê, D.; Lacovig, P.; Veselli, E.; Lizzzit, S.; Comelli, G.; Rosei, R. *J. Phys. Chem. C* **2010**, *114*, 436.

8 Wu, R.; Freeman, A. J. *Phys. Rev. B* **1995**, *52*, 12419

9 Pallassana, V.; Neurock, M.; Hansen, L. B.; Hammer, B.; Nørskov, J. K. *Phys. Rev. B* **1999**, *60*, 6146

10 Hammer, B.; Morikawa, Y.; Nørskov, J. k. *Phys. Rev. Lett.* **1996**, *76*, 2141

11 Ruban, A.; Hammer, B.; Stoltze, P.; Skriver, H. L.; Nørskov, J. K. *J. Mol. Catal. A: Chem.* **1997**, *115*, 421.

12 Andersen, J. N.; Hennig, D.; Lundgren E.; Methfessel M.; Nyholm R. and Scheffler M., *Phys. Rev. B* **1994**, *50* , 17525

13 Bianchettin, L.; Baraldi, A.; de Gironcoli, S.; Vesselli, E.; Lizzit, S.; Petaccia, L.; Comelli, G.; Rosei, R. *J. Chem. Phys.* **2008**, *128***,** 114706

14 Vesselli, E.; Baraldi, A.; Bondino, F.; Comelli, G.; Peressi, M.; Rosei, R. *Phys. Rev. B* **2004**, *70*, 115404

15 Oba, Y; Sato, T.; Shinohar, T. *Phys. Rev. B* **2008**, *78*, 224417

16 Hüger, E.; Osuch, K. *Europhys. Lett.* **2003**, *63*, 90

17 Alexandre, S. S.; Anglada, E.; Soler, J. M.; Yndurain, F. *Phys. Rev. B* **2006**, *74*, 054405

18 de Siervo, A.; De Biasi, E.; Garcia1, F.; Landers, R.; Martins, M. D.; Macedo, W. A. A. *Phys. Rev. B* **2007**, *76*, 075432

19 McCavish, N. D.; Bennett, R.A *Surf. Sci.* **2003**, *546*, 47

20 Bennett, R. A.; Mulley, J. S.; Newton, M. A.; Surman, M. *J. Chem. Phys.* **2007**, *127*, 1

21 Shih, H. D.; Jona, F.; Jepsen, D. W.; Marcus, P. M. *J. Phys. C: Solid State Phys.* **1976**, *9*, 1405

22 http://www.reading.ac.uk/web/FILES/chemistry/Georg_Held_LEED_Description.pdf

23 Held, G.; Braun, W. *CLEED manual*, available from the authors

24 Pendry, J. B. *Low Energy Electron Diffraction*: Academic Press: London, 1974.

25 Van Hove M. A.; Tong, S. Y. *Surface Crystallography by LEED*: Springer: Berlin, 1979.

26 Supporting Information.

27 Pendry, J. B. *J. Phys.* **1980**, *C 13*, 937

28 de la Figuera, J.; Puerta, J. M.; Cerda, J.I.; El Gabaly, F.; McCarty, K. F. *Surf. Sci.* **2006**, *600*, L105

29 Somorjai, G. A. *Introduction to surface chemistry and catalysis*: Wiley: New York, 1994

30 http://www.casaxps.com/

31 Witten Jr., T. A.; Sander, L. M. *Phys. Rev. Lett.* **1981**, *47*, 1400

32 Röder, H.; Bromann, K.; Brune, H.; Kern, K. *Phys. Rev. Lett.* **1995**, *74*, 3217

33 Barbieri, A; Jentz D.; Materer N.; Held, G.; Dunphy J.; Ogletree D.F.; Sautet P.; Salmeron M.; Van Hove, M.A.; and Somorjai, G.A. *Surf. Sci*. **1994,** *312,* 10

34 Felter, T. E.; Sowa, E. C.; Van Hove, M. A. *Phys. Rev. B: Cond. Matt.* **1989**, *40*, 891

35 Baraldi, A.; Bianchettin, L.; Vesselli, E.; de Gironcoli, S.; Lizzit, S.; Petaccia, L.; Zampieri, G.; Comelli, G. and Rosei, R. *New J. Phys*. **2007**, 9, 143.

TOC